Image Cover Sheet

CLASSIFICATION	SYSTEM NUMBER
UNCLASSIFIED	499704

TITLE

IMPLEMENTATION OF ELASTIC-PLASTIC AND FRACTURE CAPABILITIES IN IFSAS

System Number:

Patron Number:

Requester:

Notes:

DSIS Use only:

Deliver to:

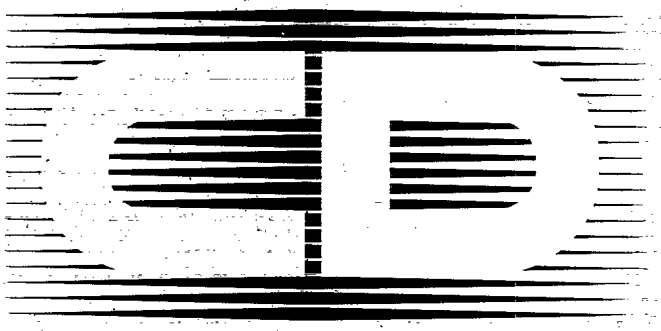

COMBUSTION DYNAMICS LTD.

Implementation of Elastic-Plastic and Fracture Capabilities in IFSAS

by

Combustion Dynamics Ltd.
Medicine Hat, Alberta
CANADA T1A 8B5

April 12, 1996

CONTRACT NO. W7701-5-3990/001-XSK

DREV SCIENTIFIC AUTHORITY
C. FORTIER
(418) 844-4279

TABLE OF CONTENTS

1.0 Introduction

Blast waves induced by mines and military explosives can cause large deformations and strains in military metal structures. These strains can cause stress levels in the metal that exceed the yield strength by a considerable margin, resulting in permanent damage to the structure. If the damage levels are severe enough, the metal may rupture, and therefore lose all load carrying capability. The fracturing of materials in non-solid media (gas, liquid) may cause jetting at the fracture points. This may help propagate the fracture due to large pressures at the fracture locations. If a numerical model is adopted to predict structural response in non-solid media, the selection of an appropriate stress-strain (or constitutive) model is of paramount importance. Assuming mechanical behavior only (no thermal dependence), the following characteristics are significant in the large deformation of metals:

1) Loss of stiffness - Figure 1.1 shows a stress-strain curve for a typical metal. After the yield strength, σ_y, is reached, the material undergoes a significant loss in stiffness. The stress increment reached is smaller for a given strain increment than before yield is reached.

2) Irrecoverable deformation - if the material is unloaded to zero stress when the yield stress is surpassed, a permanent set, or plastic deformation, is induced in the material. This is shown in Figure 1.1 as ε_p.

3) Loading-unloading (cyclic) behavior - Figure 1.2 shows a typical load cycle for a material stressed well past the first yield point in compression, and then yielded in tension. It is seen that the compressive and tensile yield stresses, σ_{yc} and σ_{yt} respectively, are not equal. This inequality of yield stresses is a function of the plastic strain in the material, and is referred to as the Bauschinger effect.

4) Fracture - the material loses all strength, and a crack or tear is formed. Physically, new surfaces form as a result of the fracture.

This report describes the implementation of an elastic-plastic fracturing constitutive model to simulate stress-strain behavior in metals. The elastic-plastic model adopted here is similar to one used by Krieg and Key (1976), and used by Hallquist (1983) in the dynamic finite element code DYNA3D. Stiffness changes are incorporated through use of a multilinear stress-strain curve. An elastic-plastic constitutive law with a mixed hardening flow rule is used to simulate plastic deformations and cyclic loading effects. Fracturing is incorporated by using a maximum effective plastic strain model described later.

This report is divided into three further sections. Section 2 provides a description of the model, and implementation details. Section 3 describes the incorporation of a fracture model within the context of the fluid-structure interaction code IFSAS. Finally, Section 4 is a description of a large deformation problem analysed using an in-house solid hydrocode.

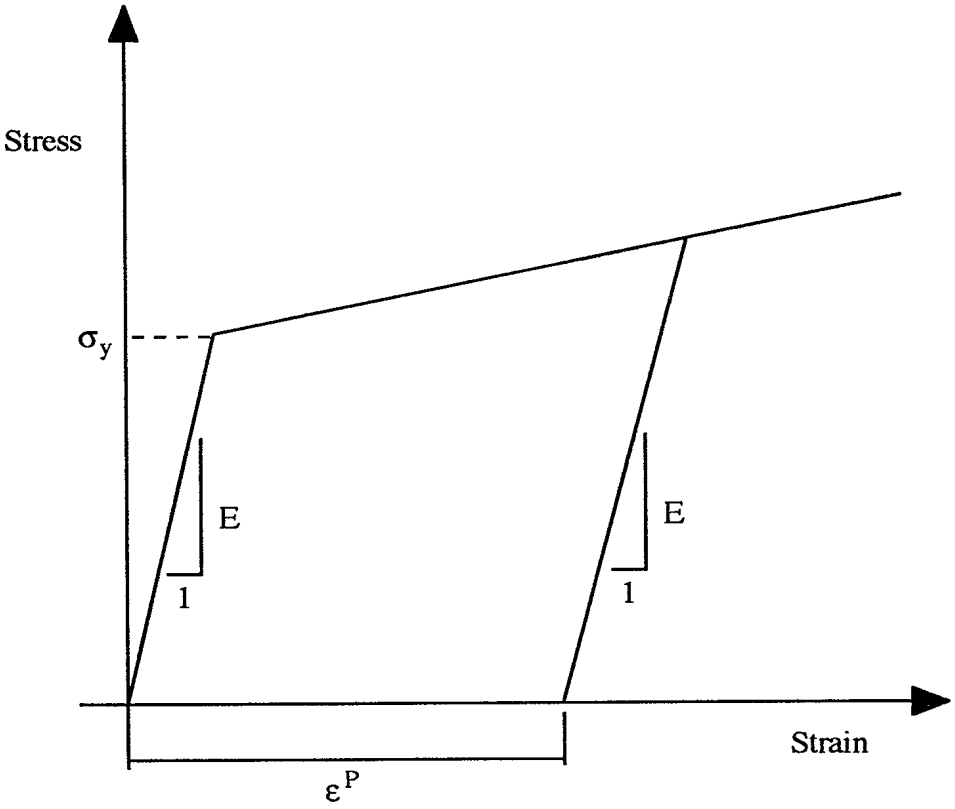

Figure 1.1 Typical stress-strain curve

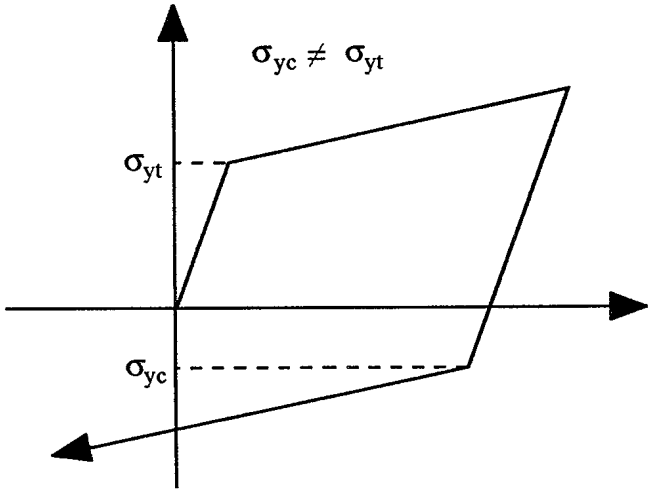

Figure 1.2 Bauschinger effect

2.0 Elastic-Plastic Model

2.1 Preliminaries

Before describing the implementation details of the elastic-plastic model, it is instructive to describe some of the fundamentals of plasticity theory. In addition to the elastic properties of the material, three properties are necessary to characterize the material behavior:

1) Yield condition - this specifies the state of multiaxial stress corresponding to the start of plastic deformation.

2) Flow rule - this relates the plastic strain increments to the current stresses and the stress increments subsequent to yielding.

3) Hardening rule - this specifies how the yield condition is modified during plastic deformation.

For most metals, the yield condition is adequately described using a multiaxial surface referred to as a Von Mises yield surface. Figure 2.1 shows the surface in two and three dimensional states of stress. This can be described mathematically as:

$$F(\sigma_{ij}, \sigma_y) = 0 \qquad [2.1]$$

where i and j are tensorial notation throughout this section. The form of the function will be described later in the implementation details.

It has been experimentally determined that plastic deformations cause little or no volume changes in metals. This means that plastic deformations are a function of the distortional strain energy only, i.e. of the deviatoric stresses. This is represented schematically in Figure 2.2. The direction of the plastic strain increments is in the same direction as the normal to the yield surface (parallel to the deviatoric stress axis), and is represented as:

$$d\varepsilon_{ij}^{P} = \frac{\partial F}{\partial \sigma_{ij}} d\lambda \qquad [2.2]$$

Equation 2.2 is the standard form for what is referred to as an associated flow rule.

In metals, there are two basic hardening rules in widespread use: isotropic and kinematic hardening. The cases of isotropic and kinematic hardening are shown in Figures 2.3 and 2.4 respectively. In the case of isotropic hardening, the compressive and tensile yield stresses σ_{yc2} and σ_{yt2} are equal, but larger than the initial yield stress. This is achieved by expanding the yield surface isotropically. For kinematic hardening, the yield surface is assumed to maintain the same radius throughout loading. To simulate uneven yield strengths, the yield surface is translated in the direction of loading.

Most metals exhibit behavior between these two models, although kinematic hardening is usually more dominant. However, it seems advantageous to include both models if possible.

2.2 Krieg and Key Model - Implementation

The model adopted here is similar to that proposed by Krieg and Key (1976), and the implementation procedure is taken from Hallquist (1983). Incorporation of a mixed isotropic-kinematic hardening rule is achieved by varying a parameter called β. For $\beta = 0$ and 1, respectively, kinematic and isotropic hardening are obtained. The yield condition and hardening rule are incorporated in the yield surface equation:

$$F = \frac{1}{2}\xi_{ij}\xi_{ij} - \frac{\sigma_y^2}{3} = 0 \qquad [2.3]$$

where

$$\xi_{ij} = s_{ij} - \alpha_{ij} \qquad [2.4]$$

$$s_{ij} = \sigma_{ij} - \frac{1}{3}\sigma_{kk}\delta_{ij} \qquad [2.5]$$

$$\sigma_y = \sigma_o + \beta E_P \varepsilon_{eff}^P \qquad [2.6]$$

$$E_P = \frac{E_T E}{E - E_T} \qquad [2.7]$$

s_{ij} = stress deviator coordinates of the current stresses
α_{ij} = stress deviator coordinates of the center of the yield surface
δ_{ij} = Kroenecker delta
E = elastic modulus
E_T = tangent modulus
E_P = plastic modulus
σ_o = initial yield stress

The implementation of the Krieg and Key model proceeds as follows for a given time step:

1) Calculate a trial elastic stress increment Δs_{ij}^*, and update the total stresses to a trial stress state s_{ij}^*

$$\Delta s_{ij}^* = 2G\Delta\varepsilon_{ij}' \qquad [2.8]$$

$$\Delta\varepsilon_{ij}' = \Delta\varepsilon_{ij} - \frac{1}{3}\Delta\varepsilon_{kk}\delta_{ij} \qquad [2.9]$$

$$G = \frac{E}{2(1 - \nu)} \qquad [2.10]$$

G = shear modulus
ν = Poisson's ratio

2) Evaluate the yield function, F, from Equations 2.3 and 2.4

$$F = \frac{3}{2}\xi_{ij}\xi_{ij} - \sigma_y^2 \qquad [2.11]$$

The yield stress, σ_y, is evaluated as a multilinear function of the effective plastic strain, ε_{eff}^P, as shown in Figure 2.5. The effective plastic strain is used to describe a six-dimensional plastic strain state as an "equivalent" uniaxial strain state. In this manner, uniaxial stress strain curves provide enough data for a complete description of the multiaxial strain state.

3) If $F < 0$, the stress state is in the elastic range, and the stress update is completed. If $F > 0$, the material has yielded, and additional steps are taken. Compute the increment in effective plastic strain, $\Delta\varepsilon^P$, and update the total effective plastic strain

$$\Delta\varepsilon_{eff}^P = \frac{\left(\frac{3}{2}\xi_{ij}^*\xi_{ij}^*\right)^{1/2} - \sigma_y}{3G + E_P} \qquad [2.12]$$

$$\varepsilon_{eff}^{P^{n+1}} = \varepsilon_{eff}^{P^n} + \Delta\varepsilon_{eff}^P \qquad [2.13]$$

4) If yielded, the stress deviators s_{ij}^* are not coincident with the yield surface as indicated by Equation 2.3. Therefore, these must be scaled on to the yield surface.

$$s_{ij}^{n+1} = s_{ij}^* - \frac{3G\Delta\varepsilon_{eff}^P}{\left(\frac{3}{2}\xi_{ij}^*\xi_{ij}^*\right)^{1/2}}\xi_{ij}^* \qquad [2.14]$$

5) If some kinematic hardening occurs ($\beta < 1$), the yield surface has translated. The center coordinates, α_{ij}, must be updated.

$$\alpha_{ij}^{n+1} = \alpha_{ij}^n + \frac{(1-\beta)E_P\Delta\varepsilon_{eff}^P}{\left(\frac{3}{2}\xi_{ij}^*\xi_{ij}^*\right)^{1/2}}\xi_{ij}^* \qquad [2.15]$$

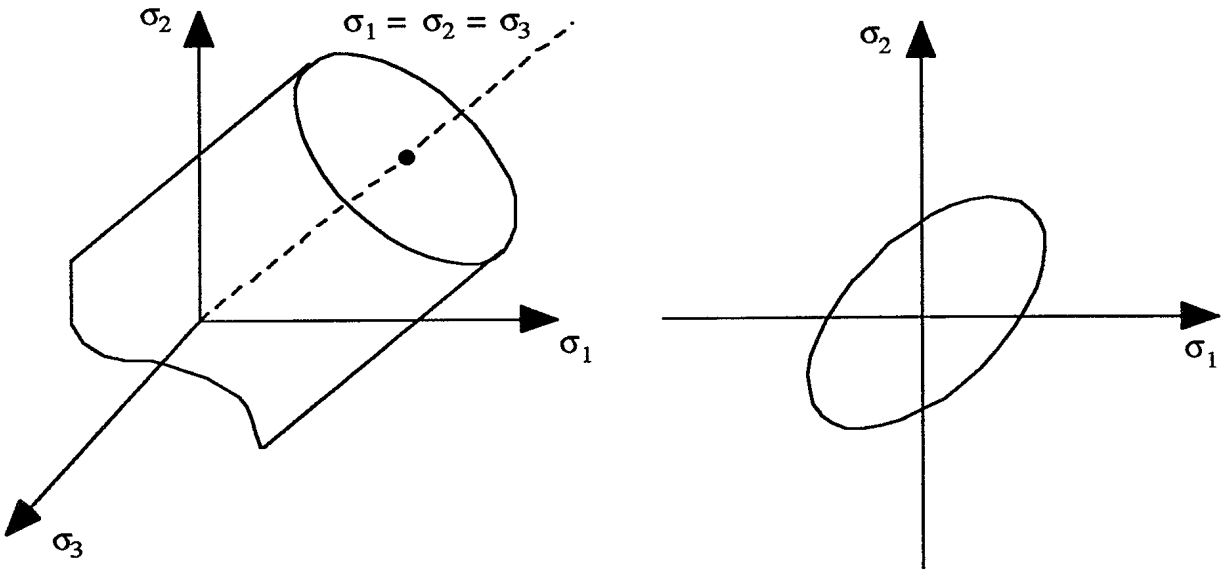

Figure 2.1 Von Mises yield surface

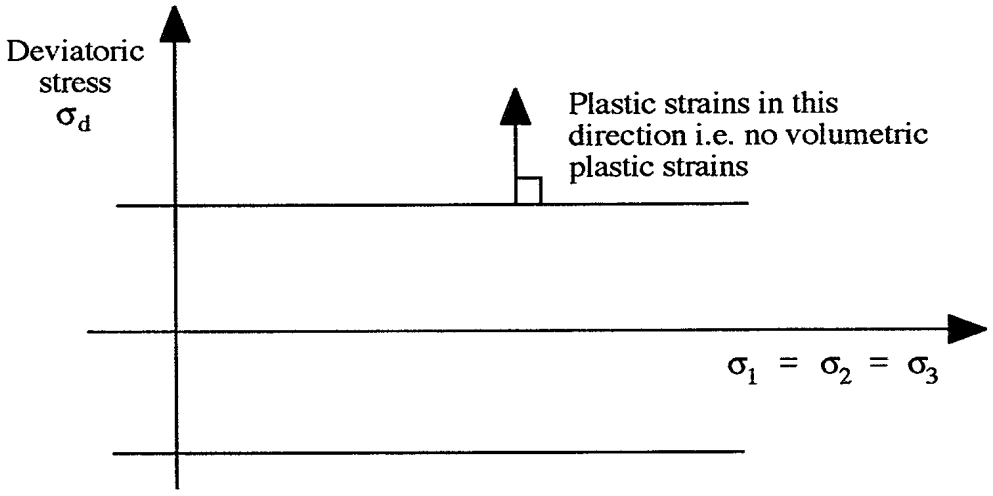

Figure 2.2 Plastic strain increments

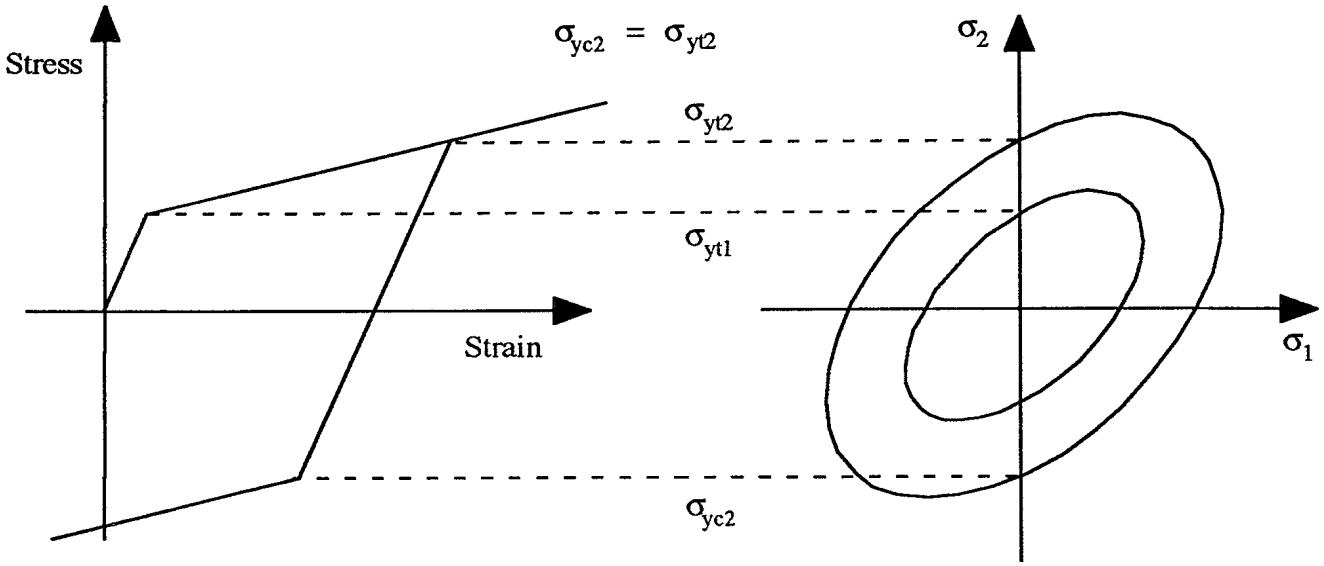

Figure 2.3 Isotropic hardening

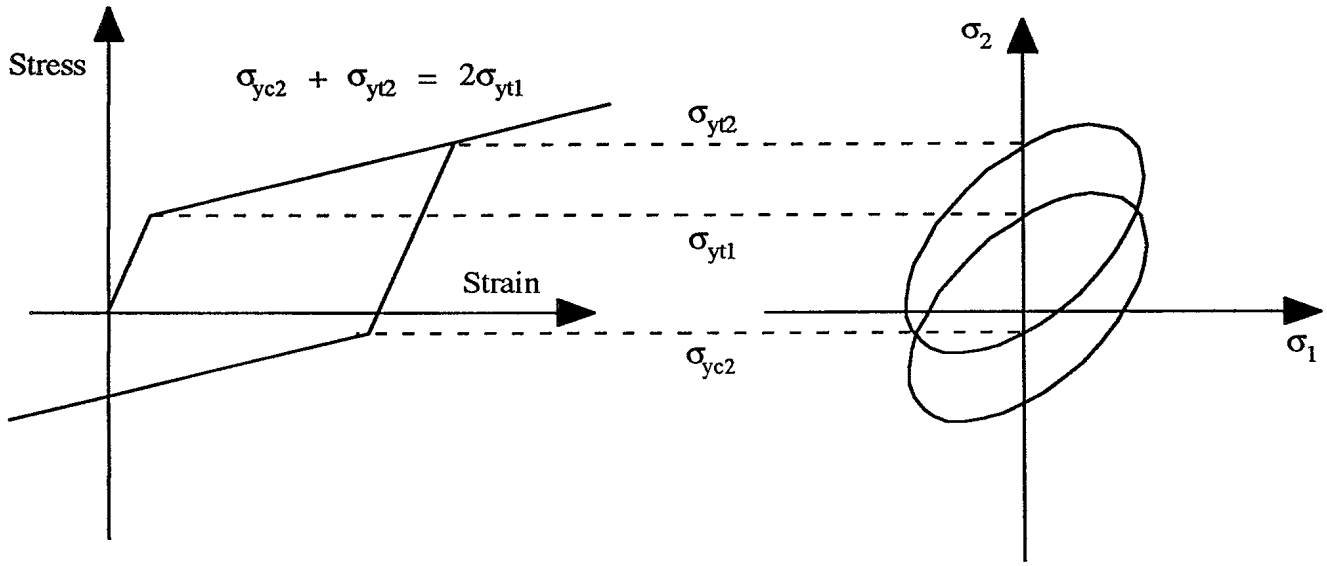

Figure 2.4 Kinematic hardening

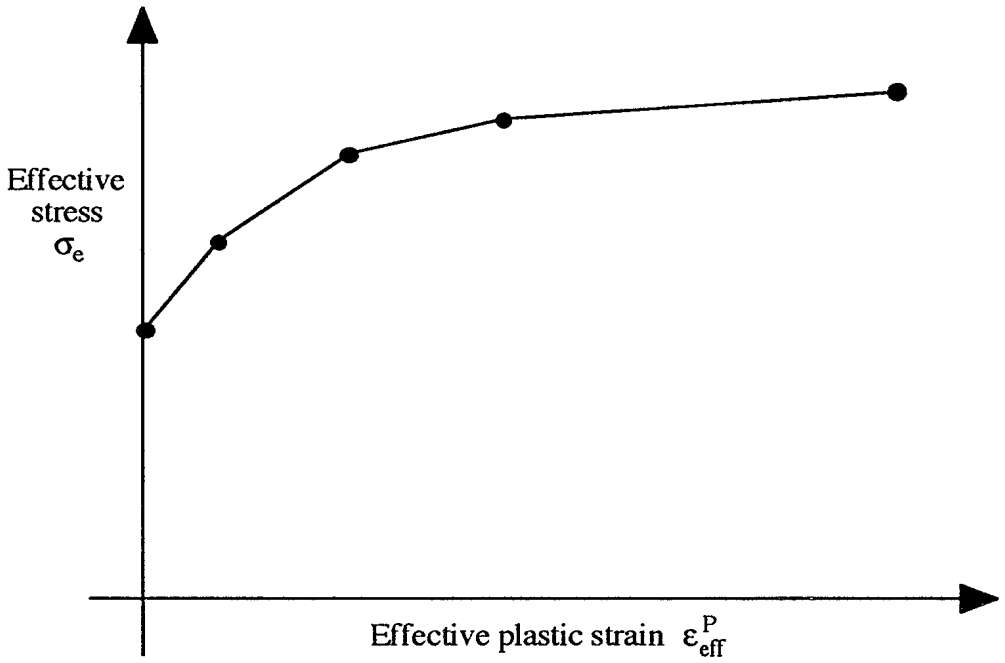

Figure 2.6 Multilinear stress-strain curve

3.0 Implementation of Fracture Model Into IFSAS

Currently, IFSAS uses a coupled Lagrange-Euler formulation to solve fluid-structure interaction problems. The approach can be seen schematically in Figure 3.1. Pressures from the Eulerian CFD code are used by the Lagrangian solid code to compute the displacements and velocities of the solid. These kinematic variables are used by the CFD code to update the fluid pressures, and the cycle continues until the analysis end.

Given this formulation type, incorporation of a fracture model into the fluid-structure interaction code IFSAS can be divided into the following parts:

1) Fracture identification - a criterion is required to determine whether the solid has fractured.

2) Solid hydrocode treatment of fracture - the formation of fracture voids must be allowed.

3) CFD treatment - the fracture causes modifications in the solid shape, which must be accommodated in the CFD code.

3.1 Fracture Identification

In recent years, the method of fracture identification used by many solid hydrocodes (finite element, finite difference) is the maximum effective plastic strain model. This model assumes that when the maximum effective plastic strain is reached on the effective uniaxial stress-strain curve, fracture occurs. This is equivalent to saying that once the maximum plastic internal work is reached at a continuum point, fracture occurs. Fracture is assumed independent of the stress path i.e. compressive or tensile fracture is possible.

The model adopted here is similar to the one described above, with a slight modification. It is assumed that fracture cannot occur if the continuum point is under compressive stresses. The hydrostatic (or average) stress component, σ_h, is a measure of this, and is given by the expression

$$\sigma_h = \sigma_{kk}/3 \qquad [3.1]$$

If $\sigma_h > 0$, the stress state is in volumetric tension (conducive to fracture). Thus, the condition for fracture is defined as

$$\varepsilon_{eff}^{P} \geq \left(\varepsilon_{eff}^{P}\right)_{max} \qquad [3.2]$$

$$\sigma_h \geq 0 \qquad [3.3]$$

If Equations 3.2 and 3.3 hold at any point in the solid, fracture is identified at that point.

3.2 Solid Hydrocode Treatment

Once fracture is identified, modifications must take place within the material model calculations. Since fractured metals have no strength either in tension or compression, no stress can be sustained across the fractured point. The stress calculations are typically performed at one

point near the centroid of the element. Once fracture occurs, the stresses are set to zero at this point, which is the same as saying that the element is removed. An easier method to implement this element removal is to include a fracture (or death) flag in the element information. Once this flag has been switched on, the element is ignored in the stress and load vector calculations.

An additional consideration is the formation of new pressure surfaces due to fracture voids. Since the solid hydrocode is coupled to an Euler CFD code, identification of all pressure surfaces in contact with the fluid is critical. Figure 3.3 shows an example of the creation of new fracture surfaces in the solid. Firstly, the lower left element is identified as having fractured. Next, the element is removed from the element stress and load vector calculations. Finally, the new free surfaces are identified so that the CFD code can properly identify the shape on the Euler grid.

It is not completely certain yet as to what scheme is to be adopted for identification of new free surfaces. It may be possible to identify all internal and external line surfaces, and then use the surfaces that only contain one element line. The line surfaces would be updated throughout the calculation.

3.3 CFD Code Treatment

Once the new pressure surfaces have been determined, the solid is ready to be located on the grid. The location is performed as previously done in the IFSAS code, with one exception. It is possible to create empty cells due to void formation in the solid. These cells must be filled with material from the adjoining cells. It is possible to fill these cells by using the average of a given quantity of cells adjacent to the empty ones, or by using an advection scheme.

3.4 Fracture Algorithm Summary

The following steps are necessary to incorporated fracture within a Lagrangian-Eulerian formulation:

1) Solid calculation

   a) Perform stress calculation for each element, and identify the fractured cells. If cells are previously fractured, ignore them in the stress and pressure surface calculations.

   b) Identify all new pressure surfaces caused by the element fracture, and present to the CFD code in a form it can understand.

2) CFD calculation

   a) Given the new solid fracture surfaces, place the new shape on the grid.

   b) Fill any empty cells caused by void formation or solid movement.

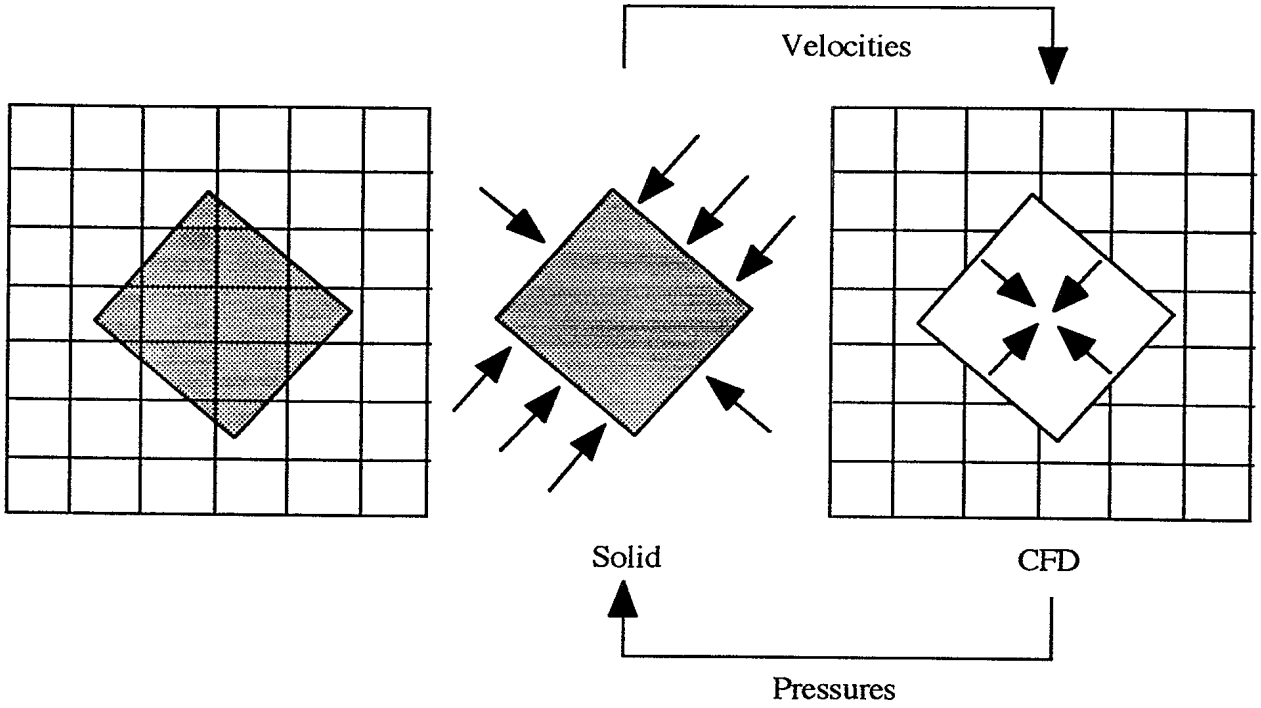

Figure 3.1 Coupled Lagrange-Euler formulation

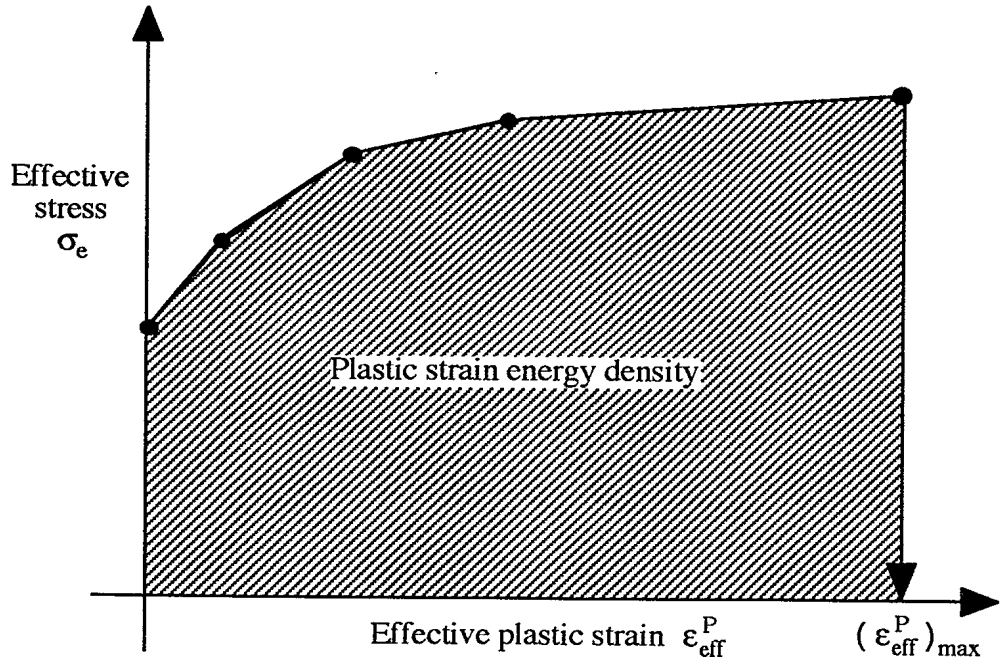

Figure 3.2 Maximum effective plastic strain fracture model

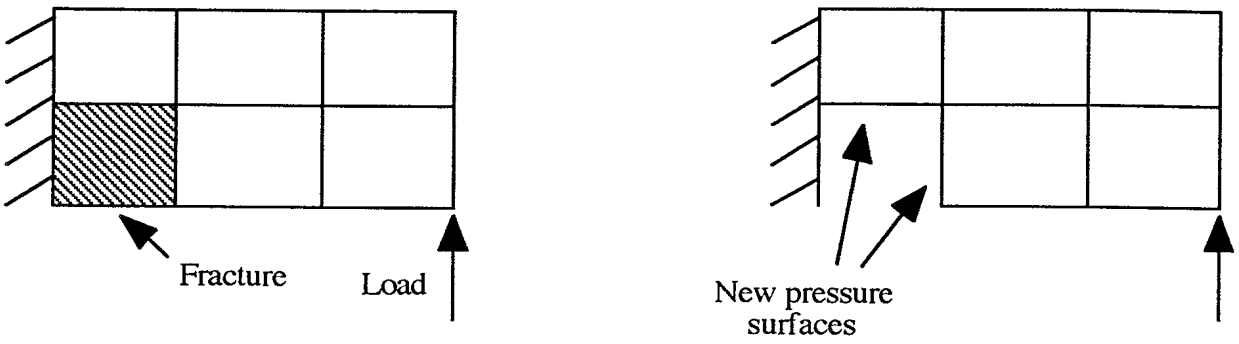

Figure 3.3 Fracture voids

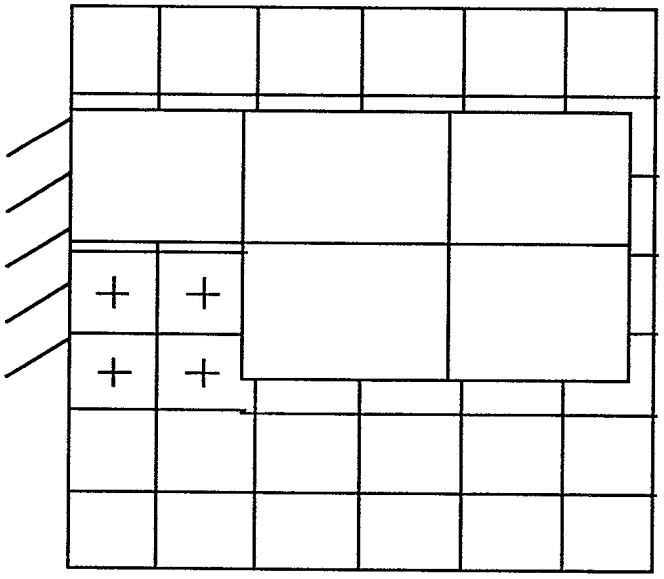

+ Empty cells

Figure 3.4 Empty cell creation

4.0 Large Deformation Example Problem

In order to demonstrate the large deformation capability of the elastic plastic model described in Section 2.0, an example problem was analysed using an explicit in-house code. The model consists of a bullet-like solid impacting a rigid wall at 700 m/sec, and is shown in Figure 4.1. The model was axisymmetric, with imposed initial velocities of 0.0 m/sec at the wall surface, and 700.0 m/sec everywhere else. The solid was given material properties which are consistent with some high strength steels. An isotropic hardening rule was assumed here. Large deformations are incorporated using an updated Lagrangian Jaumann formulation similar to that described by Bathe (1982) and Hallquist (1983).

Figure 4.2 shows the deflected shape of the cylinder at the analysis end time of 4.9×10^{-5} sec. At this point, if the cylinder was assumed to move as a rigid body, the y-coordinate of the top surface should be 0.0157 m. The top coordinate is greater than this at approximately 0.029 m because the bullet is slowed by the impact against the wall. It can also be seen that the bullet flares out at the point of impact, nearly doubling in radius, and that the top surface has moved to approximately 3/5 of its original height. The analysis terminated when the maximum failure strain of 2.0 mm/mm was reached. The displaced shapes are qualitatively similar to a 3-D analysis performed by Goudreau and Hallquist (1982). No direct comparison was possible due to the lack of numerical data.

No problems were encountered in the solution of this problem. The analysis was performed on a PowerMac, and was completed from start to finish in approximately 2-3 minutes for 700 time steps.

To summarize, analysis of the bullet produced results qualitatively consistent with other investigators. The finite element model was able to accommodate extremely large deformations with no computational difficulties, thereby implying high model stability. The calculation was performed on a personal computer in a relatively short time; this implies that the finite element model is competitive with other solution schemes, such as implicit finite element or finite difference. It remains to validate the model with experimental data.

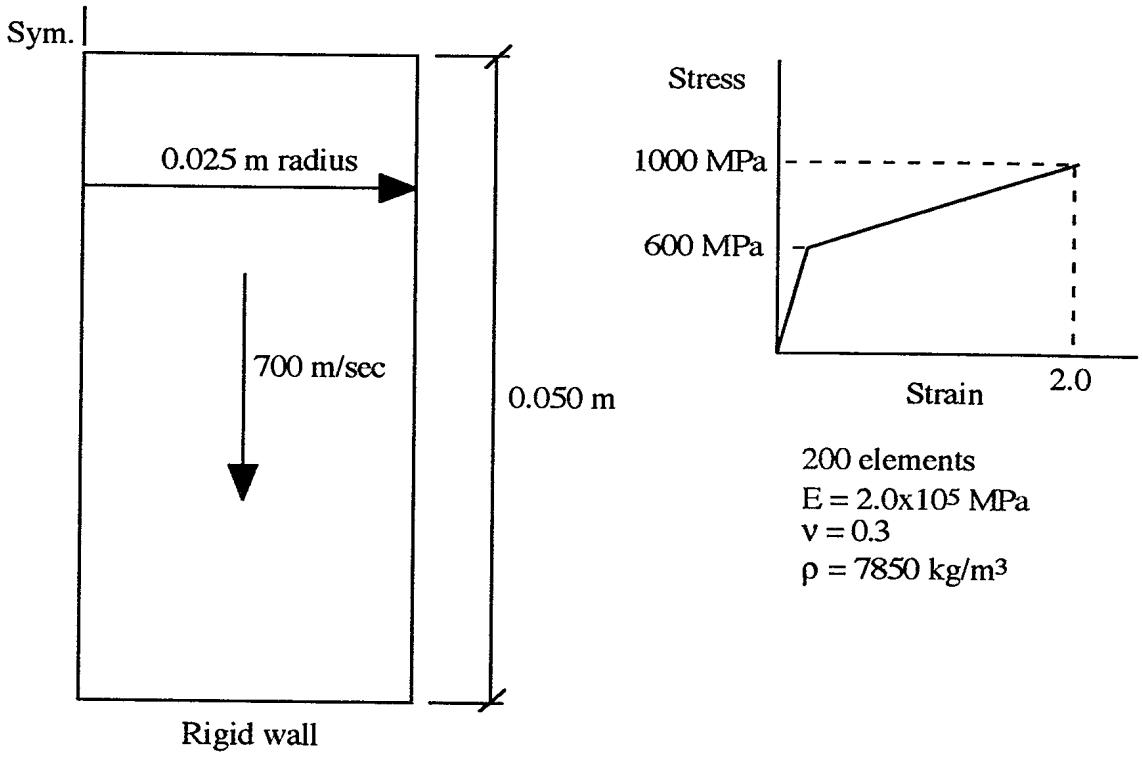

Figure 4.1 Axisymmetric finite element model of bullet

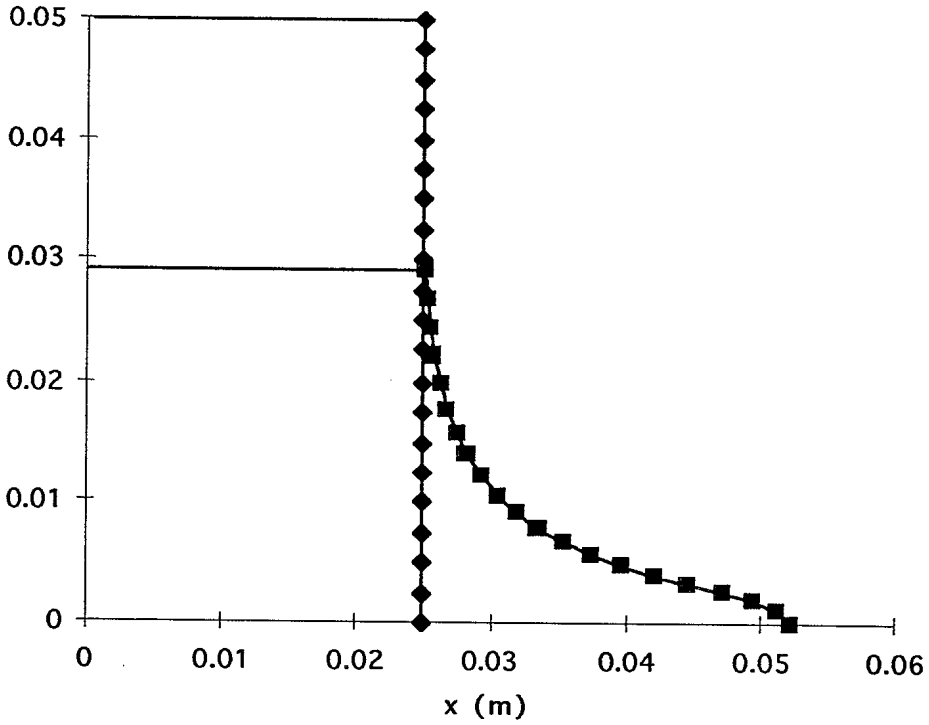

Figure 4.2 Deflected vs. initial shape at 4.9X10-5 sec

5.0 References

Hallquist, J.O. (1983). Theoretical Manual for DYNA3D. Lawrence Livermore Laboratory, Report UCID 19401, 82 p.

Bathe, K. J. (1982). Finite Element Procedures in Engineering Analysis. Prentice-Hall, 735 p.

Goudreau, G.L., and Hallquist, J.O. (1982). Recent Developments in Large Scale Finite Element Lagrangian Hydrocode Technology. Computer Methods in Applied Mechanics and Engineering, v. 33, pp. 725-757.

Krieg, R.D., and Key, S.W. (1976). Implementation of a Time Dependent Plasticity Theory into Structural Computer Programs. Constitutive Equations in Viscoplasticity: Computational and Engineering Aspects, v. 20, American Society of Mechanical Engineers, New York, N.Y., pp 125-137.

NO. OF COPIES NOMBRE DE COPIES	COPY NO. COPIE N°	INFORMATION SCIENTIST'S INITIALS INITIALES DE L'AGENT D'INFORMATION SCIENTIFIQUE
1	1	BA
AQUISITION ROUTE FOURNI PAR ▶		DREV
DATE ▶		23 Oct 96
DSIS ACCESSION NO. NUMÉRO DSIS ▶		

DND 1158 (6-87)

National Defence / Défense nationale

499704

PLEASE RETURN THIS DOCUMENT TO THE FOLLOWING ADDRESS:

DIRECTOR
SCIENTIFIC INFORMATION SERVICES
NATIONAL DEFENCE
HEADQUARTERS
OTTAWA, ONT. - CANADA K1A 0K2

PRIÈRE DE RETOURNER CE DOCUMENT À L'ADRESSE SUIVANTE:

DIRECTEUR
SERVICES D'INFORMATION SCIENTIFIQUES
QUARTIER GÉNÉRAL
DE LA DÉFENSE NATIONALE
OTTAWA, ONT. - CANADA K1A 0K2